16th International Conference on Space Operations, Cape Town, South Africa – 3 - 5 May 2021.


SpaceOps-2021,7,x1630

# Bearing-Only Navigation to Support Proximity Operations on Cislunar Non-Keplerian Orbits

**Michele Ceresoli***, **Giovanni Zanotti**†, **Michèle Lavagna**‡
Dipartimento di Scienze e Tecnologie Aerospaziali (DAER), Politecnico di Milano, Italy

**Abstract**

In the near future many space missions will exploit the cislunar domain to advance and develop the technologies required to bring humans on Mars. The Lunar orbital Platform Gateway (LOP-G) will play a key role as a deep-space outpost but will require rendezvous and docking/undocking capabilities to safely operate and connect with other spacecraft. While non-keplerian dynamics has been exploited by different stand-alone robotic missions in both the Earth-Moon and the Sun-Earth systems, no autonomous proximity operation has been experienced so far in that regime. In this framework, the goal of the present research is to demonstrate the applicability of the so-called Bearing-Only technique to perform relative navigation in the cislunar environment. A novel quasi-autonomous architecture based on a Shrinking Horizon – Model Predictive Control (SH-MPC) is developed to compute the guidance profile and favour the target observability with angles-only measurements. A computationally efficient dynamical formulation is adopted to allow the exploitation of the same architecture in both small satellites and large spacecraft. The ability of this Guidance, Navigation and Control (GNC) scheme to navigate from the far-range to precise hovering points is assessed with a numerical testing campaign and sensitivity analyses. The outcomes highlight the effectiveness of the proposed architecture and its ability to meet traditional safety and navigation requirements in most of the cislunar space domain.

**Keywords**: Rendezvous Optimisation, Relative Non-Keplerian Dynamics, Bearing-only Navigation, Shrinking Horizon Model Predictive Control

**Abbreviations**

| | | | |
|---|---|---|---|
| DRO | Distant Retrograde Orbit | QP | Quadratic Programming |
| NLP | Non Linear Programming | SH | Shrinking Horizon |
| NRHO | Near Rectilinear Halo Orbit | SQP | Sequential Quadratic Programming |

## 1. Introduction

The last decade has experienced a worldwide consolidation of numerous Moon related space missions to develop and advance the technologies required for a future exploration of Mars. Among those, NASA's Artemis program plays a dominant role, aiming to bring back humans on the lunar surface by the mid-20s. In this framework, the Lunar Orbital Platform Gateway (LOP-G) will play a critical part as a long-term modular infrastructure, supporting activities on and around the Moon. The activities on the Gateway and on the lunar surface will be supported by various space transportation systems which will deliver cargo, experiments, and logistics. To enable and safely accomplish these assembly and re-supply missions, autonomous rendezvous and docking/undocking capabilities must be consolidated. In particular, although a great deal of experience on Guidance, Navigation and Control (GNC) techniques for rendezvous in Low Earth Orbit (LEO) has been gained through the International Space Station (ISS) programme, no proximity operation has been autonomously performed so far in the non-keplerian regime.

This paper focuses on assessing the applicability of already known approaches to perform proximity navigation on Earth orbits, to the NRHO LOP-G case. In particular, the so-called Bearing-Only technique is here selected as potentially available, from a sensor suite perspective, on all spacecraft classes, from nano to large sats. Bearing-Only navigation estimates the relative state of an observer through angular measurements of the line-of-sight vector only. Although this technique requires simple, cheap, and lightweight navigation sensors, its application in the space environment has been sparsely studied because of inherent limitations in estimating the range.

Recently, in the context of in orbit relative motion Woffinden [1] and Grzymisch [2] have proved that a necessary and sufficient condition for observability is the execution of maneuvers that yield a difference of at least one measurement between the perturbed trajectory and its evolution if no maneuvers had occurred. In addition, the former author proposed a metric based on the relative range and the observability angle but analytical solutions were only found for very simple cases [3]. On the other hand, Grzymisch [4] quantified the observability through the positive linear independence of the relative position vector with a maneuver and that of the natural evolution and has shown

*MSc Candidate, michele.ceresoli@mail.polimi.it
†PhD Candidate, giovanni.zanotti@polimi.it
‡Full Professor, michelle.lavagna@polimi.it

the possibility of combining the same observability metric with a fuel objective to obtain a Quadratic Programming (QP) optimisation problem [5]. More recently, Mok [6] developed a one-step guidance which exploits the Fisher Information Matrix (FIM) to quantify and enhance the observability in a closed-loop architecture. Nevertheless, little to no literature exists regarding the applicability of bearing-only navigation to perform proximity operations in non-keplerian orbits.
Therefore the goal of the present paper is to develop a novel approach to favour the target observability while respecting traditional rendezvous requirements in the cislunar domain. In Section 2 the geometry of the bearing-only problem is presented and is followed in Section 3 by a detailed description of the mathematical formulation behind the proposed GNC architecture. Finally, in Sections 5 and 6 the simulation results are presented and few final considerations are reported in Section 7.

## 2. Problem Definition

The geometry of the bearing-only range detectability is well illustrated by Fig. 1, where the target (the grey circle) is fixed in the origin of the system and the chaser position is depicted before and after the observable maneuver (red circles). The angle $\theta$ is called the observability angle and is the angle between the natural and true Line-Of-Sight (LOS) vectors. In the ideal scenario (i.e., perfect measurements) the relative distance $\rho$ can be directly found through the law of sines, however, the sensor readings will always be affected by some kind of noise $\varepsilon$, leading to an inherent uncertainty $\delta\rho$ in the range estimation. These could be due to pixel misreadings or to errors in the image processing algorithms.

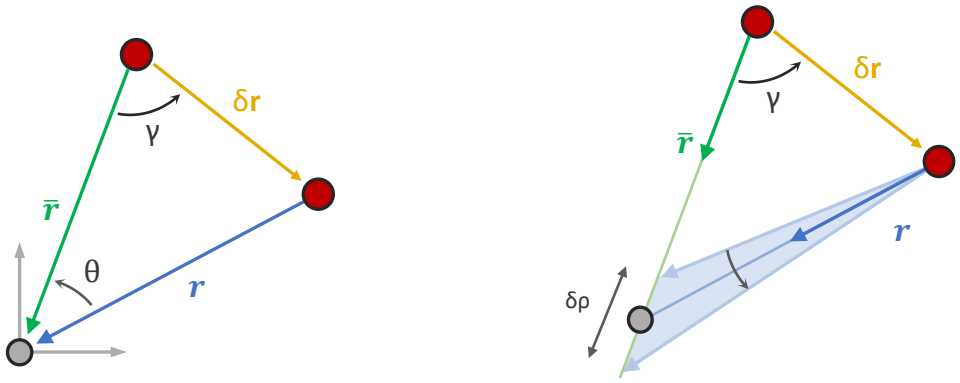


Figure 1: Range detectability geometry in the ideal (*left*) and real (*right*) scenario. $\mathbf{r}$ is the position vector of the real trajectory whereas $\bar{\mathbf{r}}$ represents the natural dynamics. Image readapted from [3].

For typical rendezvous applications, a useful design parameter is the relative range uncertainty. According to Woffinden [3], under the assumption of small measurement errors, this metric is expressed as:

$$\frac{\delta\rho}{\rho} = \frac{\varepsilon}{\sin\theta} \tag{1}$$

Therefore, there are two distinct ways to minimise the uncertainty. The first is to improve the sensor accuracy. However, there are physical and technological limitations to the minimum achievable value for $\varepsilon$. In addition, one of the major benefits of bearing-only solutions is that they only require a camera to work, meaning great economic savings in terms of hardware and requiring very accurate sensors would simply deny them any advantage. Thus, this criterion clearly shows that in order to reduce the relative range estimation error, the design of the trajectory should focus on maximising the observability angle $\theta$. The following section illustrates how the observability angle can be included inside the design of the rendezvous trajectory to favour the target observability.

## 3. Shrinking Horizon Bearing-Only Guidance

When dealing with a bearing-only architecture, the navigation process is directly influenced by the shape of the trajectory, therefore, it is mandatory to include inside the trajectory design a contribution that allows to improve the navigation performance. In this work, a Shrinking Horizon – Model Predictive Control (SH-MPC) is selected to compute the maneuvers required to bring the spacecraft to a desired location. In this formulation, the trajectory is discretised into a series of points, arbitrarily spaced in time. However, differently from a standard MPC approach [7], with a shrinking horizon the rendezvous duration is fixed, and the problem is always solved from the current epoch until the final time, thus the time window shrinks at each re-optimisation according to the remaining rendezvous time. The course of action for this kind of architecture is displayed in Fig. 2. Calling $T_{rdv}$ the desired

rendezvous time, the trajectory is discretised into $n$ steps $t_M = [t_{M_1}, t_{M_2}, ..., t_{M_n}]$ and at each of those a maneuver is allowed. At the same time, the number $m$ of reoptimisation performed along the trajectory is scheduled for $t_O = [t_{O_1}, t_{O_2}, ..., t_{O_m}]$ and is such that $t_{O_i}$ does not necessarily equal $t_{M_i}$. Once the guidance is initialised, for each update time $t_j$ it checks whether an optimisation is planned at the current epoch. If that is the case, the minimisation algorithms sets the estimated relative state as the initial point and searches a solution for the remaining discretisation points, eventually updating the maneuver scheme $\mathbf{U}_{opt}$. Afterwards, it also controls if a maneuver is planned; whenever that is the case, the chaser executes the control action according to $\mathbf{U}_{opt}$. Finally, the cycle is stopped when $T_{rdv}$ is reached.

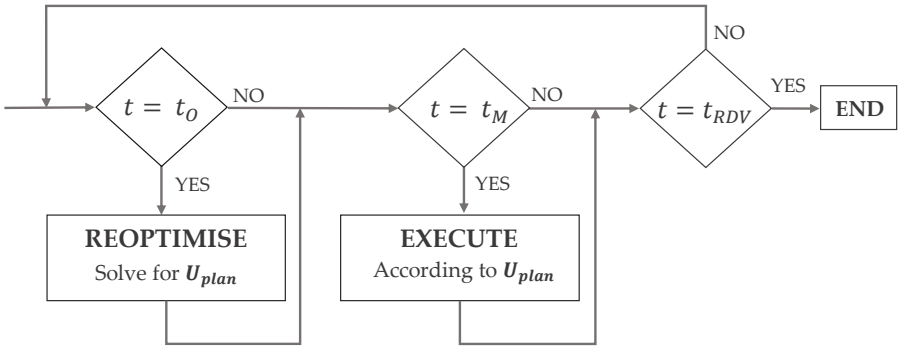


Figure 2: Guidance Flow-chart.

Please notice that in a real implementation, it might not be feasible to solve the optimisation problem and execute a maneuver at the exact same epoch. Nevertheless, it is here assumed that the two tasks can be accomplished simultaneously.

### *3.1. Dynamic Model*

An object in the cislunar space domain is influenced by the gravitational potential of both Moon and Earth and by the perturbing effects of the Sun's gravitational force and the Solar Radiation Pressure (SRP). Considering a formulation based on the Circular Restricted Three Body Problem (CR3BP), the absolute dynamics of the cislunar domain can be approximated in the inertial frame as:

$$\mathbf{f}(\mathbf{x}) = \begin{cases} \ddot{x} = -\dfrac{(1-\mu)(x+\mu)}{r_1^3} - \dfrac{\mu(x-1+\mu)}{r_2^3} + a_{4th_x} + a_{SRP_x} \\ \ddot{y} = -\dfrac{(1-\mu)y}{r_1^3} - \dfrac{\mu y}{r_2^3} + a_{4th_y} + a_{SRP_y} \\ \ddot{z} = -\dfrac{(1-\mu)z}{r_1^3} - \dfrac{\mu z}{r_2^3} + a_{4th_z} + a_{SRP_z} \end{cases} \tag{2}$$

The equations have been expressed in non-dimensional form through $\mu$, i.e., the mass parameter of the Earth-Moon system. The terms $r_1$ and $r_2$ are the spacecraft distances from Earth and Moon, respectively. The relative translational dynamics is easily obtained by differentiating the definition of the relative position vector of the chaser with respect to the target, denoted as $\mathbf{x}$:

$$\ddot{\mathbf{x}} = \ddot{\mathbf{r}}_c - \ddot{\mathbf{r}}_t \tag{3}$$

Where $\ddot{\mathbf{r}}_c$ and $\ddot{\mathbf{r}}_t$ are the absolute acceleration vectors of the two spacecraft. To allow the exploitation of traditional linear control theory techniques for the design of the trajectory profile, the relative dynamics in Eq. (3) can be linearised with respect to the target position by applying a first-order Taylor expansion, under the assumption that the relative distance between the spacecraft is much smaller than the distance between the target and the primaries [8]:

$$\begin{bmatrix} \dot{\mathbf{x}} \\ \ddot{\mathbf{x}} \end{bmatrix} \approx \begin{bmatrix} \mathbf{0} & \mathbf{I}_3 \\ \boldsymbol{\Xi}(t) & \mathbf{0} \end{bmatrix} \begin{bmatrix} \mathbf{x} \\ \dot{\mathbf{x}} \end{bmatrix} + \begin{bmatrix} \mathbf{0} \\ \mathbf{I}_3 \end{bmatrix} (\mathbf{u} + \delta\mathbf{a}) = \mathbf{A}(t) \begin{bmatrix} \mathbf{x} \\ \dot{\mathbf{x}} \end{bmatrix} + \mathbf{B}(\mathbf{u} + \delta\mathbf{a}) \tag{4}$$

Where $\mathbf{I}_3$ a $3 \times 3$ identity matrix, $\mathbf{u}$ is the control input and $\delta\mathbf{a}$ is the contribution of the environmental perturbing accelerations. The matrix $\boldsymbol{\Xi}(t)$ depends only on the absolute position of the target (which is in turn function of time), and is defined as:

$$\boldsymbol{\Xi}(t) = -\left(\frac{1-\mu}{r_{T_1}^3} + \frac{\mu}{r_{T_2}^3}\right)\mathbf{I}_3 + 3\frac{1-\mu}{r_{T_1}^3}\left[\hat{\mathbf{r}}_{T_1}\hat{\mathbf{r}}_{T_1}^{\mathrm{T}}\right] + 3\frac{\mu}{r_{T_2}^3}\left[\hat{\mathbf{r}}_{T_2}\hat{\mathbf{r}}_{T_2}^{\mathrm{T}}\right] \tag{5}$$

where $\hat{\mathbf{r}}_{T_1}$ and $\hat{\mathbf{r}}_{T_2}$ identify the relative inertial unit position vectors between the target and the two primaries. Notice that the propagation of the relative dynamics always requires the knowledge of the relative variables and the absolute state of either the chaser or the target. This characteristic is a fundamental difference with respect to classical LEO relative dynamics models, which require knowledge of only the 6 relative states. The system of equations in Eq. (5) does not make any assumption on the model used to propagate the dynamics; thus, it can be straightforwardly adapted to work either in the CR3BP or with the ephemeris model by changing the expression of the primaries position vectors.
A closed form solution to Eq. (4) system does not exist since $\mathbf{A}$ is dependent on the absolute dynamics of the target, which requires a numerical integration. Nevertheless, given $\mathbf{x}(t_0)$ and $\mathbf{u}(t)$ the solution of Eq. (4) can be separated into a free and forced contribution as:

$$\mathbf{x}(t) = \mathbf{\Phi}(t, t_0)\mathbf{x}(t_0) + \int_{t_0}^{t} \mathbf{\Phi}(t, \tau)\mathbf{B}\mathbf{u}(\tau)d\tau \tag{6}$$

where $\mathbf{\Phi}$ denotes the State-Transition Matrix (STM) and satisfies:

$$\dot{\mathbf{\Phi}}(t, t_0) = \mathbf{A}(t)\mathbf{\Phi}(t, t_0) \quad \text{and} \quad \mathbf{\Phi}(t_0, t_0) = \mathbf{I}_6 \tag{7}$$

The solution of the forced response is more complicated and only in few cases the convolution integral of the time-varying maneuver $\mathbf{u}(t)$ can be written as the product between a matrix and a vector. For impulsive controls at the beginning of the time interval, the input matrix $\mathbf{G}(t, t_0)$ can be computed as $\mathbf{G}(t, t_0) = \mathbf{\Phi}(t, t_0)\mathbf{B}$. Once that is available, the discrete-time solution of the relative dynamics over the time interval $[t_k, t_{k-1}]$ is given by:

$$\mathbf{x}(t_k) = \mathbf{\Phi}(t_k, t_{k-1})\mathbf{x}(t_{k-1}) + \mathbf{G}(t_k, t_{k-1})\mathbf{u} \tag{8}$$

A remarkable difference with respect to classic relative models, such as the Clohessy-Wiltshire (CW) equations, other than the inexistence of an analytical solution is that the model in Eq. (4) is a time-varying linear system, thus: $\mathbf{\Phi}(t_k + \Delta t, t_k) \neq \mathbf{\Phi}(t_i + \Delta t, t_i)$ if $t_i \neq t_k$ because the dependence of $\mathbf{\Phi}$ on the target state generates different results for different initial times since $\mathbf{x}_t(t_i) \neq \mathbf{x}_t(t_k)$. Therefore, it is necessary to compute $\mathbf{\Phi}$ at each discretisation time even if a uniform time-step is adopted. However, from a computational standpoint, the exact evaluation of $\mathbf{\Phi}$ and $\mathbf{G}$ could be too burdensome as it requires the integration of 42 differential equations at each update time. For this reason, in this work inside the navigation and guidance algorithms, the STM is approximated with a 2nd order Taylor series as:

$$\mathbf{\Phi}(t_k + \Delta t, t_k) = \mathbf{I}_6 + \mathbf{A}_k\Delta t + (\mathbf{A}_k^2 + \dot{\mathbf{A}}_k)\Delta t^2/2 \tag{9}$$

With $\mathbf{A}_k$ used to indicate the value of $\mathbf{A}(t)$ at time $t_k$.

### *3.2. Optimisation Problem*

The optimisation problem solved at each re-optimisation epoch is written in the form of:

$$\begin{aligned} \min_{\mathbf{y}} \quad & \mathcal{J}_F(\mathbf{y}) \\ \text{subject to} \quad & \mathbf{A}_{eq}\mathbf{y} = \mathbf{b}_{eq} \\ & \mathbf{A}_{iq}\mathbf{y} \leq \mathbf{b}_{iq} \\ & \mathbf{l}_b \leq \mathbf{y} \leq \mathbf{u}_b \\ & c(\mathbf{y}) \leq 0 \end{aligned} \tag{10a}$$

where $\mathbf{y}$ is the vector of independent variables, containing the maneuvers directions and, possibly, other associated quantities. $\mathbf{A}_{eq}$ and $\mathbf{A}_{iq}$ are the matrices that express the equality and inequality constraints, respectively. These are used to bound the relative motion to specific regions of space and specify the boundary conditions; namely, the initial and final points of the trajectory. $\mathbf{l}_b$ and $\mathbf{u}_b$ are the lower and upper bounds for the solution space of $\mathbf{y}$ and allow to include inside the problem the system engineering limitations (e.g., the maximum thrust available). $\mathcal{J}_F$ is the objective to minimise and includes a linear expression of the fuel consumption. Finally, $c(\mathbf{y})$ is a non-linear function that constraints the observability angle at a given epoch to improve the navigation estimate.
To clarify the future notation, assuming the time-interval is discretised in $n$ points, the relative states can be collected inside a vector $\mathbf{X} = [\mathbf{x}_1^T\ \mathbf{x}_2^T\ ...\ \mathbf{x}_n^T]^T$ of size $6n \times 1$. At the same time, the maneuvers are admissible at every point but the last one, otherwise an additional relative state would be produced. Thus, in a similar fashion they are collected inside a global vector $\mathbf{U} = [\mathbf{u}_1^T\ \mathbf{u}_2^T\ ...\ \mathbf{u}_{n-1}^T]^T$ of size $3(n-1) \times 1$.

*3.2.1. Fuel Objective*

In this work, a representation of the fuel expenditure is obtained by adopting a so-called 1-norm objective; that is, the sum of the absolute values of all thrust elements inside **U**:

$$\mathcal{J}_{F_s} = \sum_{k=1}^{3(n-1)} |\mathbf{U}_k| \tag{11}$$

This class of cost function generally yields solutions with smaller $\Delta$V when compared to traditional quadratic control objectives. Additionally, the maneuver plan is characterised by sparser control actions that are quite appealing when a continuous-thrust system is not available. However, the downside of having few maneuvers is that, if the control schedule is not executed properly, the trajectory may be subject to large deviations from the original plan. The objective in Eq. (11) is a piece-wise linear function and a conversion is desirable to efficiently solve the optimisation problem with a Sequential Quadratic Programming (SQP) algorithm. Therefore, a new set of variables $\mathbf{S} = [\mathbf{s}_1^T \ \mathbf{s}_2^T \ ... \ \mathbf{s}_{n-1}^T]^T$, called slack variables [5] is introduced inside the optimisation vector **Y**. Then, by adding specific inequality constraints, each of the elements inside **S** can be set equal to the absolute value of the corresponding element in **U**. Defining $\mathbf{Y} = [\mathbf{U}^T \ \mathbf{S}^T]^T$ the augmented optimisation vector, the cost function in Eq. (11) is written as:

$$\mathcal{J}_{F_s} = \mathbf{F}^T\mathbf{Y} \tag{12}$$

where the vector **F** has the first $3(n-1)$ elements equal to zero and the remaining set to one. To ensure **S** equals the absolute value of **U** , each $j$-element must be subject to the following two constraints:

$$\begin{aligned} \mathbf{U}_j - \mathbf{S}_j &\leq 0 \\ -\mathbf{U}_j - \mathbf{S}_j &\leq 0 \end{aligned} \tag{13}$$

The system in Eq. (12) is generalised to every maneuver by expressing all the individual constraints through a matrix as:

$$\mathbf{A}_s\mathbf{Y} \leq \mathbf{b}_s \qquad \text{where} \qquad \mathbf{A}_s = \begin{bmatrix} \mathbf{I}_m & -\mathbf{I}_m \\ -\mathbf{I}_m & -\mathbf{I}_m \end{bmatrix} \quad \text{and} \quad \mathbf{b}_s = \mathbf{0}_{2m} \tag{14}$$

with $m = 3(n-1)$. Notice that, even though with non-linear solvers the 1-norm of **U** can be computed without the need of introducing slack variables, the SQP algorithm finds a solution in less time when $\mathcal{J}_F$ is a continuous and smooth function; that would not be the case if the sum of the modulus of **U** was directly computed.

*3.2.2. Boundary Conditions*

To specify a desired final point for the trajectory, the final position is written as function of the global maneuver vector **U** and of the initial conditions:

$$\mathbf{x}_n = \mathbb{G}\mathbf{U} + \mathbb{A}_{1n}\mathbf{x}_1 \tag{15}$$

where $\mathbf{x}_1$ is the initial point and $\mathbb{A}$ is defined as:

$$\mathbb{A}_{ij} = \prod_{k=i}^{j-1} \mathbf{\Phi}_k \ \text{ if } j > i \qquad \text{and} \qquad \mathbb{A}_{ij} = \mathbf{I}_6 \ \text{ if } j \leq i \tag{16}$$

and $\mathbb{G}$ is a $6 \times m$ matrix equal to:

$$\mathbb{G} = \begin{bmatrix} \mathbb{G}_1 & \mathbb{G}_2 & \dots & \mathbb{G}_{n-1} \end{bmatrix} \quad \text{and} \quad \mathbb{G}_j = \mathbb{A}_{(j+1)n}\mathbf{G}_j \tag{17}$$

The final equality constraint is written in the form of:

$$\mathbf{A}_{BC}\mathbf{Y} = \mathbf{b}_{BC} \quad \text{with} \quad \mathbf{A}_{BC} = \begin{bmatrix} \mathbb{G} & \mathbf{0}_{6\times m} \end{bmatrix} \quad \text{and} \quad \mathbf{b}_{BC} = \hat{\mathbf{x}}_{EC} - \mathbb{A}_{1n}\mathbf{x}_1 \tag{18}$$

where $\hat{\mathbf{x}}_{EC}$ is the desired final point. On the other hand, thrust magnitude constraints are easily added through the lower and upper bound vectors as:

$$\begin{aligned} \mathbf{l}_b &= -u_m \begin{bmatrix} \mathbf{1}_{1\times m} & \mathbf{0}_{1\times m} \end{bmatrix}^T \\ \mathbf{u}_b &= \ \ u_m \begin{bmatrix} \mathbf{1}_{1\times m} & \mathbf{1}_{1\times m} \end{bmatrix}^T \end{aligned} \tag{19}$$

Due to the discrete formulation of the original problem in Eq. (8), $u_m$ is expressed as a velocity and equals the maximum $\Delta$V available for each maneuver.

*3.2.3. Non-linear Observability Constraint*

The easiest and most effective approach to include the observability angle inside the optimisation problem is to augment (10) with an additional non-linear constraint, demanding that after M steps the observability angle should be greater or equal than a given threshold. The number of steps can be used as an additional tuning parameter. For example, it can be selected to ensure the error is reduced by the time the next re-optimisation occurs. Mathematically, the constraint is expressed as:

$$c(\mathbf{U}) = \theta_{THR} - \frac{\bar{\mathbf{x}}_M^T \mathbf{x}_M(\mathbf{U})}{\|\bar{\mathbf{x}}_M\| \|\mathbf{x}_M(\mathbf{U})\|} \leq 0 \tag{20}$$

where $\bar{\mathbf{x}}_M$ depends only on the initial conditions. By formulating this constraint as an inequality, the solver will automatically find the solution with the lowest fuel consumption among all the possible values of $\theta \geq \theta_{THR}$. The two vectors in the previous expression are easily computed as:

$$\begin{aligned} \bar{\mathbf{x}}_M &= \mathbb{A}_{1M} \mathbf{x}_1 \\ \mathbf{x}_M &= \bar{\mathbf{x}}_M + \mathbb{G}_M \mathbf{U} \end{aligned} \tag{21}$$

The matrix $\mathbb{G}_M$ is similar to (17) but is evaluated only up to the $(M-1)$-th term:

$$\mathbb{G}_M = \begin{bmatrix} \mathbb{G}_1 & \dots & \mathbb{G}_{M-1} & \mathbf{0} & \dots & \mathbf{0} \end{bmatrix} \qquad \mathbb{G}_j = \mathbb{A}_{(j+1)M} \mathbf{G}_j \tag{22}$$

The evaluation of the non-linear constraint can be accelerated by pre-computing these matrices.

## 4. Simulation Environment

To investigate the ability of the proposed architecture to perform a quasi autonomous bearing-only rendezvous, the Shrinking Horizon - MPC guidance is tested in a closed-loop system along with a navigation filter. Throughout the analysis, the target is always assumed to be moving on a periodic non-keplerian orbit. A southern NRHO around the Earth-Moon L2 point has been selected as a reference orbit to mimic a potential rendezvous scenario with the LOP-G. In addition, since previous researches have identified the NRHO apolune region as the most favourable area to perform the complex rendezvous and docking operations [8] [9], these simulations position both spacecraft in the same neighborhood.

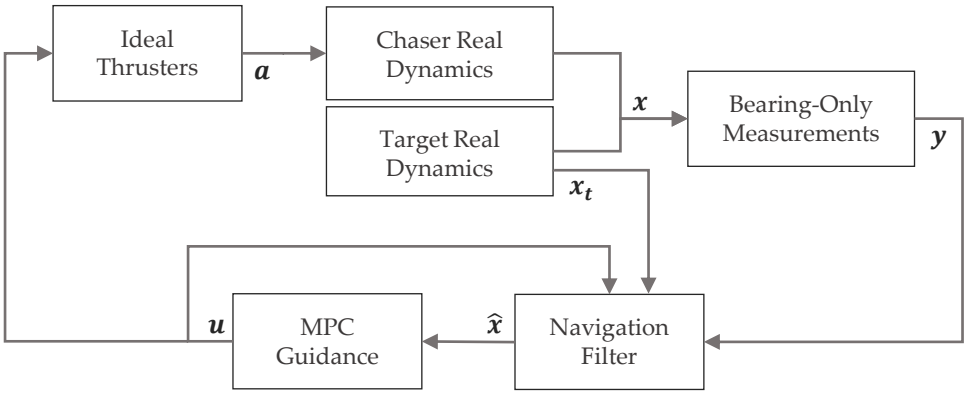


Figure 3: Simulation architecture scheme.

A scheme of the simulation architecture is presented in Fig. 3. In this framework, the guidance uses the navigation estimate for the optimisation and updates the control plan accordingly to the logic shown in Fig. 2. A high-fidelity propagator is used to simulate the chaser and target absolute dynamics, accounting for the perturbing effects of the Sun gravitational force and the SRP and exploiting NASA Spice toolbox to retrieve the position of the main celestial bodies. In this regard, the target is assumed to be a 400-tons spacecraft with an exposure area of 12.000 $m^2$, mimicking an ISS-class object. On the other hand, the chaser represents a hypothetical automated transfer vehicle, with a mass of 20 tons and total surface of 125 $m^2$.

Notice that the propagation of the relative dynamics inside the navigation filter requires knowledge of the target absolute state. For this reason, it is here supposed that at each re-optimisation epoch, an uncertain estimate of the absolute state of the target is transmitted to the chaser. Then, the information is propagated on-board until the next optimisation. Practically, the communication link could transmit the absolute states of either spacecraft, as the other is immediately available from the relative state. Unfortunately, this need for the absolute navigation makes impossible to completely automatise this guidance scheme. The control problem is not considered in this work,

thus thrusters are modelled as ideal actuators, neglecting transient states and any kind of pointing errors. An EKF is chosen as navigation filter and is aided by a Dynamic Model Compensation (DMC) to tune the state process covariance and approximate unmodelled accelerations. The propagation step is based on the model in Eq. (8), the STM is approximated according to Eq. (9) and the update frequency is set to 1 Hz. The target position with respect to the primaries is expressed in the inertial frame because it allows for a more reliable estimation than that of a rotating perspective, where the presence of cross-coupling perturbing terms is harder to model. Concerning the desired accuracy threshold, a conservative value of $0.5\%$ of the range has been chosen instead of the classical $1\%$.

## 5. Case Studies

The performance of the proposed architecture are compared with the approach of Gryzmisch [5], which is also based on a shrinking horizon guidance but it enhances observability in a different way. In particular, an observability cost function, denoted as $\mathcal{J}_o$, is exploited to enforce the positive linear independence between the natural and the perturbed position vectors. This cost function is quadratic in the optimisation variables and is combined with the fuel objective through a weighted-sum approach. The resulting problem can be solved with Quadratic Programming (QP) algorithms. The major difference with respect to the proposed approach is that $\mathcal{J}_o$ can be minimised by either changing the angle between the two vectors (i.e., $\theta$) or reducing their magnitude (i.e., moving closer to the target). To statistically characterise the navigation performance, 300 Monte Carlo simulations are run for each scenario, varying the filter initialisation and the noise effects. Two Holding Points (HP) are used to identify the desired initial and final relative states. In a practical rendezvous approach, these points are used as checkpoints: they allow to account for operational constraints by enforcing few desired relative positions throughout the approach.

### *5.1. Case A: Center Manifold*

In this scenario, the initial holding point is placed on the NRHO center manifold at a relative distance of 250 km. The natural dynamics of this location is characterised by a periodic hovering motion around the target. Therefore, it can be exploited to ensure the chaser does not drift away from the target if the control functions were to malfunction at the beginning of the rendezvous. On the other hand, to guarantee a strong passive safety, the second holding point is set on the unstable manifold at the boundary of a 1 km Keep-Out-Sphere (KOS). In a real operation, this location ensures a safe drift away from the target in case of failures [9]. The total rendezvous duration is set to 12 hours.

| **Method** | $\downarrow \Delta V$ [m/s] | $\downarrow \Delta V_R$ [-] | $\downarrow \mathrm{E}_m$ [km] | $\uparrow \mathrm{R}_{con}$ [km] | $\downarrow$NA [m] | $\downarrow$PA [m] |
|---|---|---|---|---|---|---|
| QP | 25.06 | 2.12 | 1.22 | 29.16 | **0.84** | **17.76** |
| NLP | **21.58** | **1.82** | **1.04** | **124.42** | 0.91 | 23.20 |

Table 1: Center manifold navigation performance.

$\Delta V_R$ is the ratio between the $\Delta V$ of the observability-enhanced and fuel-optimal trajectories. $\mathrm{E}_m$ is the average value of the Root Mean Square Error (RMSE) of the estimated position and $\mathrm{R}_{con}$ is the relative distance at which the filter reaches the desired accuracy. NA and PA are the final navigation and position mean errors ($1\sigma$), respectively. The arrow indicates whether the parameter should be minimised ($\downarrow$) or maximised ($\uparrow$).

The results of the simulation are visually represented in Fig. 4 and summarised in Table 1. From the left figure, it immediately stands out that the proposed formulation (NLP) provides a sudden reduction of the relative error. By directly acting on the observability angle, the maneuver performed near the 1-hour mark greatly enhances the observability of the system, causing an improvement of about 3000 m in the navigation estimate, while remaining at a relatively higher distance from the target with respect to the alternative. In this regard, the time-evolution of the range highlights the behaviour of an observability metric that includes information on the range: the QP technique favors a fast reduction of the relative distance at the cost of expensive initial impulses. However, this trajectory does not appear convenient from an operational viewpoint as the accuracy threshold is violated for most of the approach. In particular, Table 1 shows that for the formulation based on $\mathcal{J}_o$, the distance at which the filter reaches the desired accuracy is extremely close to the target because the maneuver that minimises the objective reduces the range while keeping $\theta$ very small. Thus, it is very likely that these kind of trajectories would not comply with plausible safety and navigation requirements for a rendezvous with the LOP-G. On the other hand, the non-linear approach guarantees that from approximately 125 km, the error never exceeds the 0.5% of the relative distance.

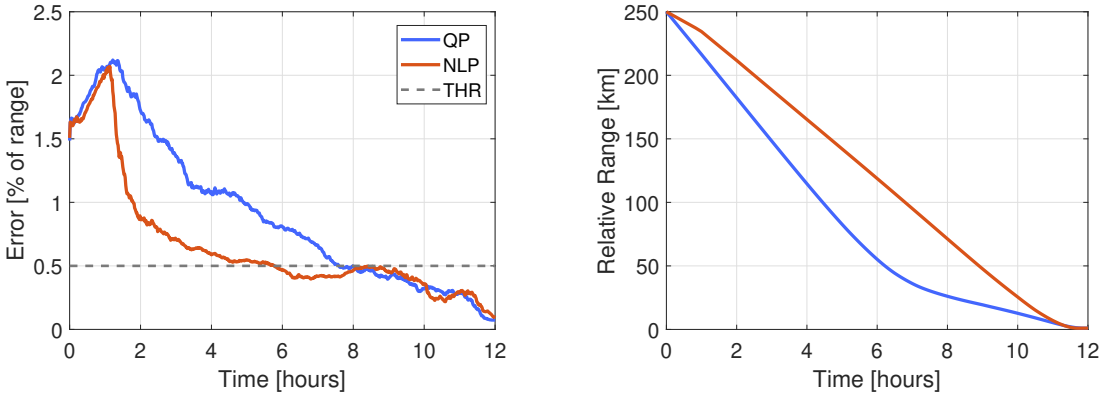


(*a*) Relative navigation error. (*b*) Relative distance.

Figure 4: Performance of the bearing-only guidance with the initial point on a center manifold

### *5.2. Case B: Quasi-Periodic Orbit*

In this test, the natural dynamics of the initial point is associated to a periodic mode of the NRHO. In particular, since the two spacecraft are on the same absolute orbit, the unperturbed motion simulates an along-track formation, with the chaser shifted backwards of an arbitrary phase angle. Instead, the final point is placed on the very same unstable manifold of the previous scenarios. The rendezvous duration is reduced to 8 hours.

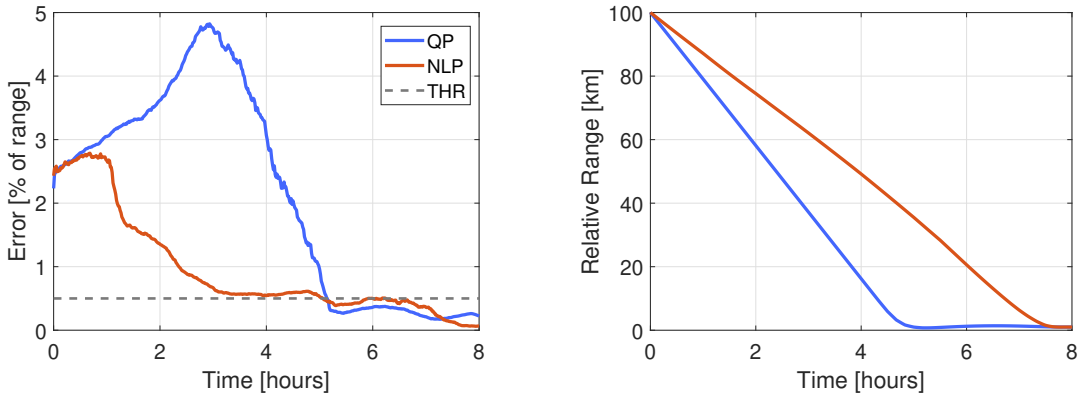


(*a*) Relative navigation error. (*b*) Relative distance.

Figure 5: Performance of the bearing-only guidance with the initial point on a quasi-periodic mode

Figure 5 presents remarkable differences with respect to the performance of the previous test. Indeed, the initial maneuvers computed with the QP objective are completely uncapable of providing an improvement in the navigation estimate for almost half of the rendezvous duration. A significant drop of the error only happens when the chaser is extremely close to the target, few hundreds of meters away from the boundary of the KOS. As a result, the relative error at 30 km is almost ten times greater than the allowed maximum.

| **Method** | $\downarrow \Delta V$ [m/s] | $\downarrow \Delta V_R$ [-] | $\downarrow \mathrm{E}_m$ [km] | $\uparrow \mathrm{R}_{con}$ [km] | $\downarrow$NA [m] | $\downarrow$PA [m] |
|---|---|---|---|---|---|---|
| QP | **12.64** | **1.77** | 1.01 | 1.03 | 2.21 | **6.81** |
| NLP | 15.51 | 2.16 | **0.67** | **34.67** | **0.67** | 25.78 |

Table 2: Periodic mode navigation performance.

$\Delta V_R$ is the ratio between the $\Delta V$ of the observability-enhanced and fuel-optimal trajectories. $\mathrm{E}_m$ is the average value of the Root Mean Square Error (RMSE) of the estimated position and $\mathrm{R}_{con}$ is the relative distance at which the filter reaches the desired accuracy. NA and PA are the final navigation and position mean errors ($1\sigma$), respectively. The arrow indicates whether the parameter should be minimised ($\downarrow$) or maximised ($\uparrow$).

Additional insights on the reasons behind the inability to reduce the error are provided by Fig. 6. The original periodic trajectory (the violet line) is characterised by an initial motion perpendicular to the $x$-$y$ plane; at the same

time, the QP formulation draws an almost straight line along the $y$-axis and thus, has minimal differences in terms of azimuth measurements with respect to the nominal trajectory. As a consequence, the filter is unable to reduce the uncertainty along the $y$-axis. The navigation estimate begins to improve only after 3 hours, when the natural motion bends towards the right-side, effectively differentiating the azimuths.

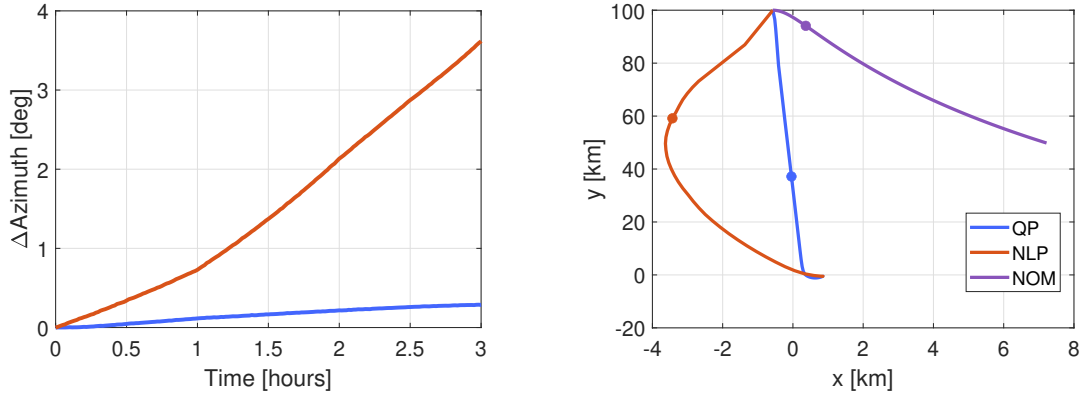


(***a***) Azimuth differences. (***b***) Trajectory projection in the $x$-$y$ plane.

Figure 6: Approaching trajectories characteristics. NOM stands for the nominal trajectory and the tiny dots represent the relative position of the chaser after 3 hours.

On the other side, the NLP guidance performs a maneuver at the 1 hour-mark that forces the chaser to move on the opposite side of they-axis, causing a sudden reduction of more than 1000 m of the navigation error. Concerning the final errors, in spite of having the best performance throughout the rendezvous, the non-linear approach has the worst position dispersion. This is associated with the absolute navigation error at the time of the last re-optimisation. Since the QP trajectories remain in close-proximity of the target for half of the rendezvous duration, they have plenty of time to reduce their absolute errors. Thus, when the final planning is performed, the navigation uncertainty is minimal. With this in mind, these two test scenario highlight that an observability metric based on $\mathcal{J}_o$ is always able to bring the chaser to the desired rendezvous point, with dispersions of only few metres. However, if standard safety and operational requirements (e.g., a threshold on the maximum percentage navigation error) are imposed, the resulting trajectories will most likely be deemed unfeasible. On the other hand, the addition of a non-linear constraint to enforce the desired observability angle has proven successful in both cases. Indeed, it consistently allowed the filter to reach convergence at reasonable distances from the target and at the same time, it had very good accomplishments in the remaining performance metrics. As a last remark, the final position dispersion can be reduced by introducing additional trajectory re-optimisations towards the ending phase of the rendezvous.

### *5.3. Observability Weights*

The previous results were obtained with a fixed observability weight $w$ for the weighted-sum optimisation. To display what happens to the quadratic observability metric (QP) $\mathcal{J}_o$ for different choices of $w$, the navigation performance for 50 different weights have been collected in Fig. 7 and 8.

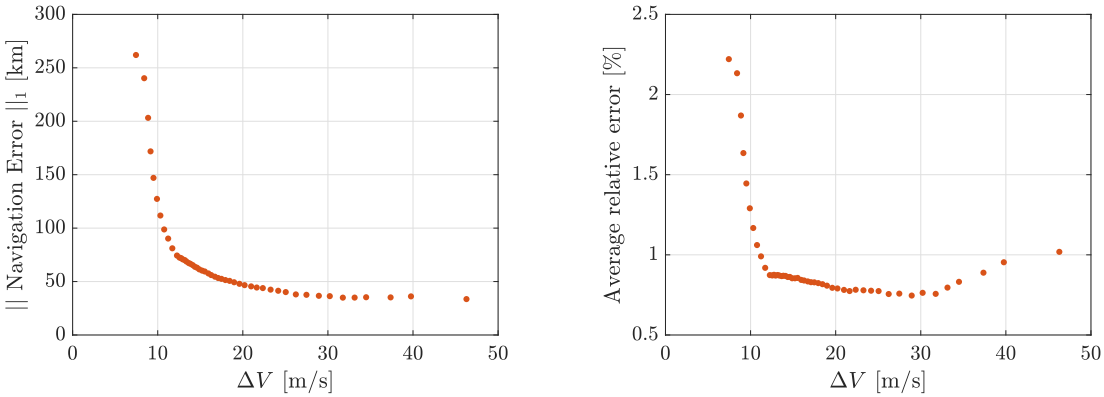


(***a***) Absolute navigation error. (***b***) Average relative error.

Figure 7: Navigation errors for increasing observability weights (i.e., for greater $\Delta V$s) for the quadratic observability objective.

Notice that each point represents the average performance of 200 Monte Carlo simulations of a rendezvous with similar settings to Case A. In addition, since increasing the observability weight favours a higher fuel consumption (see Fig. 8a), the $\Delta V$ was used in place of $w$ to aid the readability of the plots. A clear trade-off between the absolute navigation errors and the trajectory cost is visible in Fig. 7. In both plots, the points distributions resemble a standard convex Pareto curve, where small increments of $\Delta V$ lead to remarkable improvements of the navigation errors. The exact Pareto Front for the two objectives is visible in Fig. 8a and confirms that the weighted-sum approach is successful in finding the Pareto optimal solutions. However, despite increasing the observability objective effectively reduces the absolute navigation error, Fig. 8b shows that the convergence distance does not have a clear nor monotonic trend with the $\Delta V$.

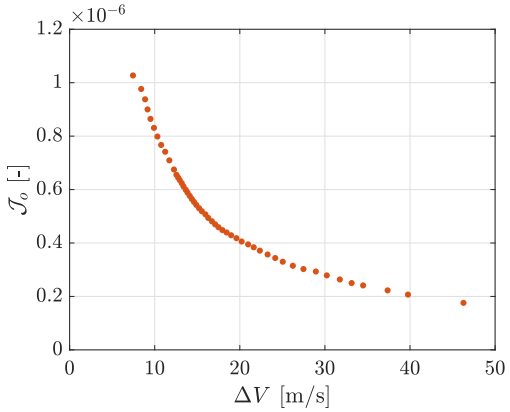


(***a***) Pareto front.

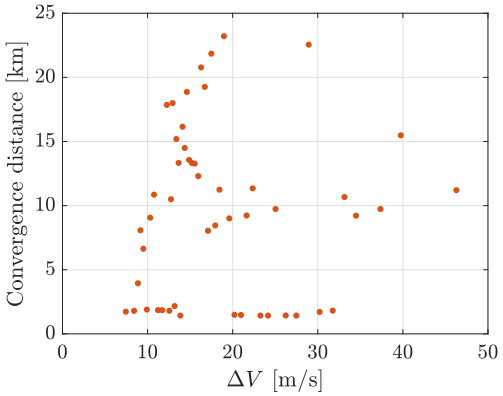


(***b***) Convergence distance.

Figure 8: Performance for increasing observability weights (i.e., for greater $\Delta V$s) for the quadratic observability objective.

Physically, increasing the observability weight generates larger initial maneuvers to move the chaser towards the final point as fast as possible. Thus, similarly to Fig. 5, the 1-norm of the absolute error is minimised at the highest $\Delta V$ because the chaser spends most of his time in close-proximity of the target. Indeed, recall from Eq. (1) that in a bearing-only application, the absolute estimation error is proportional to the relative distance. This behaviour is likely connected to the shrinking horizon formulation. In particular, by defining $\mathcal{J}_o$ as the products between all the discretisation points, the optimisation algorithm finds easier to minimise the objective by reducing as much as possible the norm of the final relative position vectors; leading to a hovering motion around the target for the remaining time.

## 6. Sensitivity Analysis

To prove the robustness of the proposed SH-MPC architecture, the navigation performance are tested over a wide range of orbital families and filter settings. Besides the importance in the field of bearing-only techniques, this analysis will also provide useful insights to aid the implementation of any type of navigation technique in the cis-lunar non-keplerian environment.

### *6.1. Filter settings*

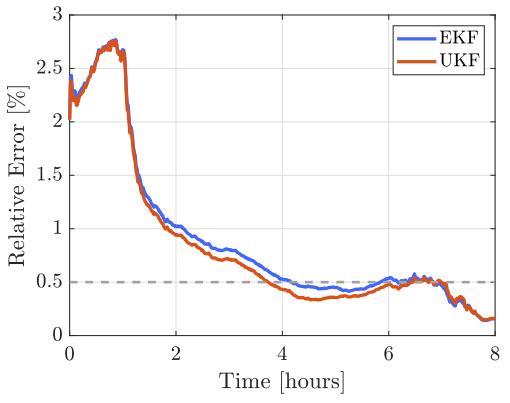


(***a***) EKF vs UKF - 1x Initial Errors.

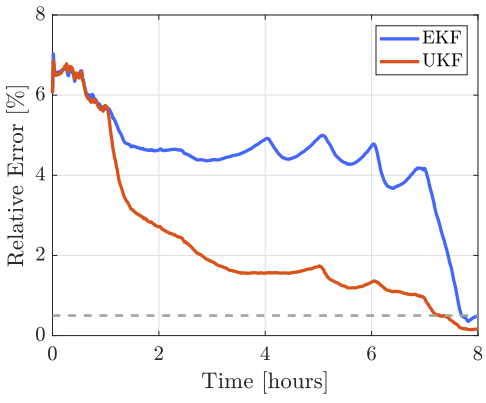


(***b***) EKF vs UKF - 3x Initial Errors.

Figure 9: Filter settings comparisons.

When applied to bearing-only navigation, one of the major limitations of the EKF in cartesian coordinates comes from the linearisation of the measurements equations, which instead are strongly non-linear. As a consequence, further inaccuracies are introduced in the estimation problem. Therefore, it is reasonable to expect an improvement in the navigation performance when an UKF is adopted. This statement is confirmed by Fig. 9, which presents the effects that different initialisation errors have on the navigation quality. The 1x initial errors correspond to a position and velocity uncertainty on each axis of 6 km and 1 m/s, respectively. The error trends show that for small initial uncertainties, the performance of the two filters are quite similar. Yet, when the initial errors increase the EKF is not able to reach convergence because it operates far from its linearisation point. On the other hand the UKF proves more robust, taking an average of 1.18 ms for each iteration with respect to the 0.21 ms of the EKF (with an Intel i7-6700 and a RAM of 16 GB). Nevertheless, for very large initial errors the accuracy threshold is violated for both filters until the chaser arrives in close-proximity of the target.

### *6.2. Target Propagation Models*

To investigate the robustness of this architecture in different orbital families, a few more considerations regarding the knowledge of the target absolute state are worth the attention. By this point, it should be well known that this information is necessary because the state transition matrix of the linearised relative dynamics depends on the motion of the target. In turn, the STM is requested by the guidance and navigation functions at each maneuver and update time, respectively. Previously, it was assumed that the information was passed at each re-optimisation epoch because an active communication link throughout the whole rendezvous might not always be available. In this regard, the chaser could directly interface with the target spacecraft, or be supported by a ground station. For example, for safety reasons it could be reasonable to assume that in a rendezvous operation, the two spacecraft can directly exchange data among themselves. Additionally, the same considerations hold when the state vector of the chaser is transmitted, as the absolute state of the target is easily obtained through the estimated relative variables. However, whenever that is the case, the target state will be affected by the same level of uncertainty of the navigation estimate and it will be harder to get accurate results. That said, once the absolute orbital information is at hand, different options are available and are summarised in Fig. 10.

Since the original linear system is time-varying and the shrinking-horizon MPC computes the trajectory from the initial time until the final one, the state information at a given epoch must be propagated on-board over the remaining sample times. Similarly to the relative motion, different levels of approximations can be exploited to compute the absolute dynamics of the target, from a simple CR3BP to a more sophisticated model based on the ephemerides. To maximise the autonomy level of the architecture, it is here assumed that the propagation must be carried out on-board. However, depending on the type of application and on the spacecraft computational resources, the same process can be performed on ground and the complete history of the trajectory is transmitted when needed. An alternative approach is available by assuming that the time-dependence of the linear system has negligible impact on the relative dynamics for short propagation times (e.g., a typical rendezvous duration). If this hypothesis holds true, the STM can be assumed constant and computed using a single value of the target state, leading to great simplifications in the assembly of the optimisation problem. However, note that the errors introduced by this approximation are also dependent on the shape of the target motion.

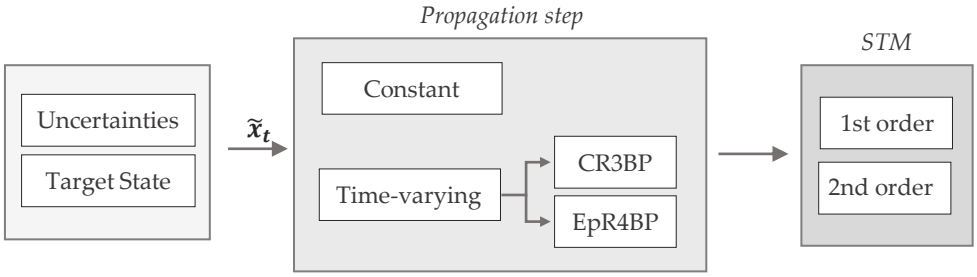


Figure 10: Target propagation approximations. This process is performed at each re-optimisation epoch.

Regardless of the propagation accuracy, the knowledge of the target absolute state is always affected by an inherent uncertainty, which impacts in different ways both the navigation and guidance algorithms. Regarding the filter, the prediction step at a generic time $t_k$ is written as:

$$\mathbf{x}_{k+1} = \mathbf{\Phi}(\mathbf{x}_{t_k})\mathbf{x}_k + \mathbf{G}_k\mathbf{u}_k \tag{23}$$

Therefore, the estimation error for $\mathbf{x}_{k+1}$ depends on the previous error at $t_k$ and on the wrong evaluation of $\mathbf{\Phi}_k$ due to the inaccuracies of $\mathbf{x}_t$ at the current time. The latter, irrespective of the propagation method, grow proportional

to the time passed from the last communication of the target state (i.e., the last re-optimisation epoch). Hence, it is to be expected that the impact of errors in the target state will be greater for longer intervals between two successive transmissions of absolute navigation data.
On the other hand, inside the optimisation problem the STM is exploited to enforce the desired boundary conditions and evaluate the observability metrics. Thus, the inexact knowledge of the target state leads to maneuvers that are incapable of either bringing the chaser to the correct destination point or providing the requested degree-of-observability. However, differently from the navigation filter, the absolute state error at any arbitrary time affects the quality of the solution, since in a SH-MPC the optimisation problem is always solved from the current epoch until the final one. Therefore, when this architecture is implemented, one should always make sure the target does not cross any regions that are characterised by a strong non-linear behaviour. Vice-versa, since in a standard MPC implementation (i.e., with a fixed horizon), the guidance only computes the relative motion over a limited window, the errors in the target dynamics should have a minor impact in the optimisation problem.
On the basis of these considerations, the performance of the proposed architecture in other cis-lunar regions will mainly depend on their numerical stability and on the ability to correctly predict the motion of the target spacecraft throughout the whole rendezvous duration.

### *6.3. NRHO Rendezvous Region*

Previous studies [8] [9] identified the NRHOs perilunes as unfeasible areas to accomplish a rendezvous, since any small perturbation of a state variable generates large deviations in the spacecraft trajectory. In this paragraph, a similar feasible rendezvous region is identified by analysing the performance of the navigation and guidance algorithms for different positions of the target along the whole NRHO. A time anomaly $\theta_t$ is used to represent the location of the target on its absolute orbit: $\theta_t = 2\pi t/T$, where $T$ is the orbital period and a null value for the anomaly identifies the aposelene of the orbit. The relative initial conditions are settled on the central manifold of each discretisation point and the rendezvous duration is fixed at 8 hours. The outcomes of the simulations are collected in Fig. 11 and 12. Note that each line is the average of 100 Monte Carlo runs.

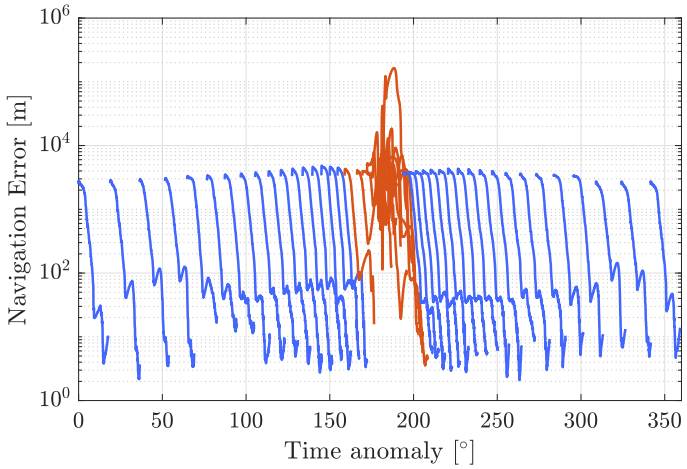


Figure 11: Navigation error evolution along a NRHO.

It stands quite clear that whenever the target moves in the region between 160 and 200 degrees, the performance of the architecture significantly deteriorate. In particular, the divergence of the navigation filter is caused by the numerical instability of the perilune region: the trajectory predicted with an uncertain relative state results remarkably different from the actual motion because of the high sensitivity to small state perturbations. Successively, the navigation divergence reflects into the inability of the guidance to define a proper maneuver plan. At each re-optimisation, the chaser finds himself in a completely wrong position and new expensive maneuvers are constantly required to adjust the trajectory.
These results are in agreement with previous studies and confirm once more that the NRHOs perilune region is not a viable candidate to perform a rendezvous. The identified ”safe” and ”forbidden” regions are depicted in Fig 13 and the red area shall be avoided as far as the proposed Bearing-Only guidance-assisted approach is adopted. In particular, since in a shrinking horizon the time of flight is a fixed design variable, the target initial conditions shall be chosen to ensure the spacecraft never reaches the unstable region throughout the whole rendezvous duration. Vice-versa, if the initial position of the target is given, the maximum rendezvous duration equals the time it takes the spacecraft to reach the boundary of the stable region.

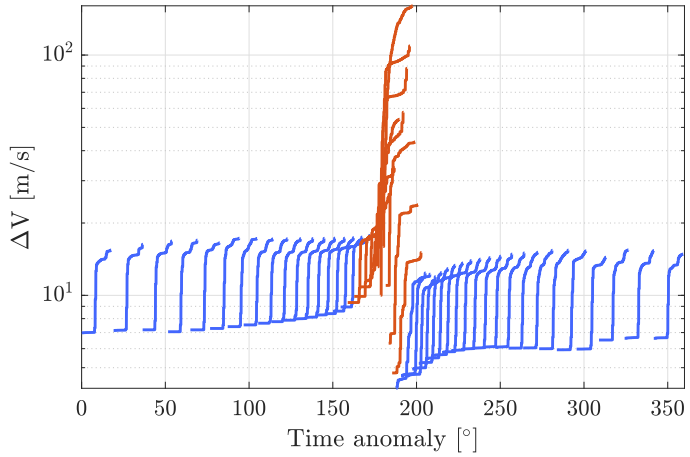


Figure 12: $\Delta V$ requirements along a NRHO.

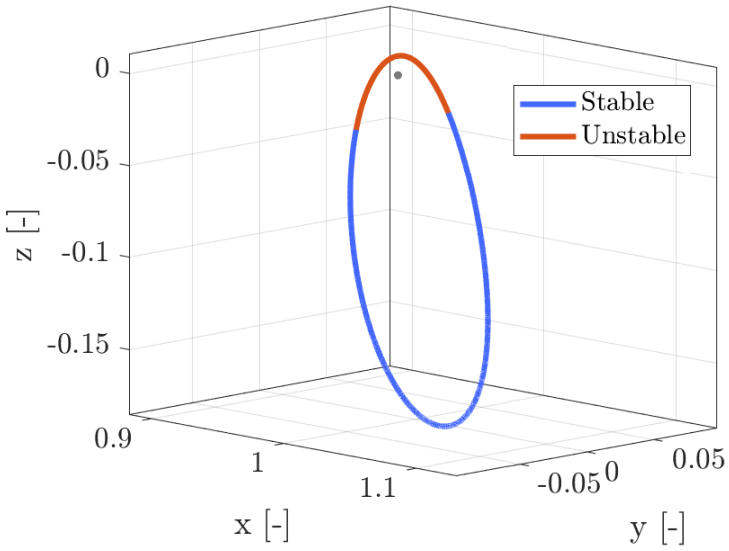


Figure 13: Suitable rendezvous region in a NRHO.

As a final remark, the performance of the GNC architecture for the different approximation techniques in Fig. 10 did not show any significant deviations with respect to those presented above. The higher accuracy of the ephemeris second order time-varying model only comes into play for close-proximity operations, where estimation errors below 1 meter are desired.

### *6.4. Time-Invariant Approximation*

A time-invariant formulation holds many benefits with respect to a time-varying model. In this framework, having a constant expression for the STM allows for an easier assembly of the optimisation problem constraints and an overall reduction of the computational effort required by the GNC functions. In addition, when only the absolute position is available, the target state cannot be propagated forward in time because its velocity is unknown, making a constant first-order STM approximation the only viable approach.

The time-dependence is associated with the variations of the relative position vectors of the target with respect to the primaries. Four different time-contributions are identifiable in Eq. (5): the magnitudes of the vectors $r_{T_{1/2}}$ and their directions (i.e., the unit vectors $\hat{\mathbf{r}}_{T_{1/2}}$). As the focus is on the cislunar domain, it is reasonable to assume that the variations of the Earth-related terms are negligible because of the much higher distance with respect to the Moon. A proper criterion to establish when the approximation holds is found by evaluating the correlation between the navigation error and the time derivatives of both $r_{T_2}$ and $\hat{\mathbf{r}}_{T_2}$; namely, the range-rate and the rotation velocity of the vector.

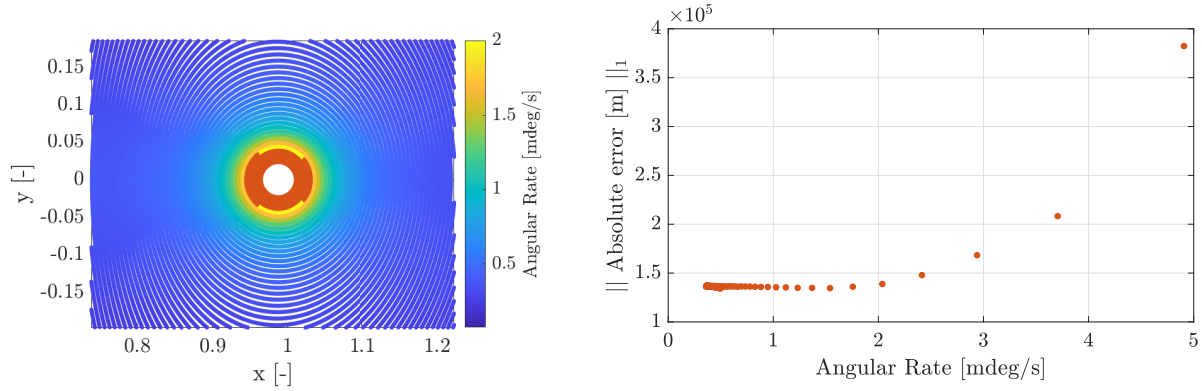


(***a***) DRO.

(***b***) Time-invariant model validity criterion.

Figure 14: Correlation between the angular rate of change of $\hat{\mathbf{r}}_{T_2}$ and the navigation error in a family of DROs. The red markers identify the regions where the time-invariant validity threshold is violated.

Using as a baseline the family of DROs in Fig. 14a, for each orbit a rendezvous approach based on a constant STM approximation was simulated and the 1-norm of the navigation errors is shown in Fig 14b as function of the angular rate of change of $\hat{\mathbf{r}}_{T_2}$. A deterioration of the navigation performance happens for angular speeds higher than 2 mdeg/s, which correspond to the innermost orbits highlighted in red in Fig. 14a. All the remaining simulations are clustered together, meaning that for lower angular rates, the time-invariant approximation does not affect in a significant way the estimation error. On the other hand, no evident correlation was found between the range-rate and increments of the navigation errors, suggesting that for the cislunar orbital families a criterion based on the angular rate of $\hat{\mathbf{r}}_{T_2}$ is enough to identify the validity regions for the time-invariant approximation.
The investigation has been expanded to other relevant families in the cislunar domain, as shown in Fig. 15 and 16. The regions where the approximation does not hold are all associated to the close-passages of the spacecraft around the Moon, such as in the NRHOs perilunes. Interestingly, the red areas of the L1/L2 Lyapunov families exhibit the same kind of numerical instability mentioned in the previous section. Indeed, regardless of the propagation method, the proposed architecture is never able to accomplish a safe rendezvous in those areas. Therefore, Fig. 15 and 16 also identify the regions were a rendezvous operation shall be avoided with the GNC scheme under study (i.e., the red areas). Viceversa, it is well known that DROs are particularly stable orbits and indeed, any kind of time-varying approximation is accurate enough to perform proximity operations even in the innermost orbits.

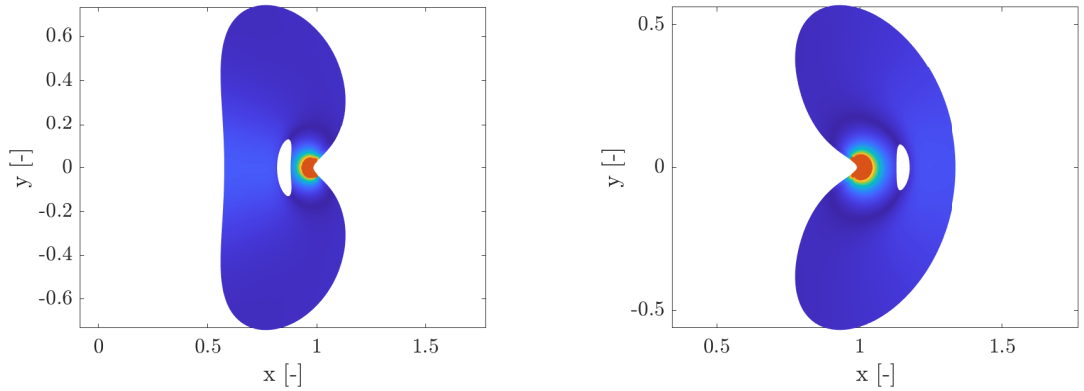


(***a***) Lyapunov L1.

(***b***) Lyapunov L2.

Figure 15: Angular rate of change of $\hat{\mathbf{r}}_{T_2}$ in the L1/L2 CR3BP Lyapunov families. The red markers identify the regions where the time-invariant validity threshold is violated. The color scale is associated to the same values of Fig. 14.

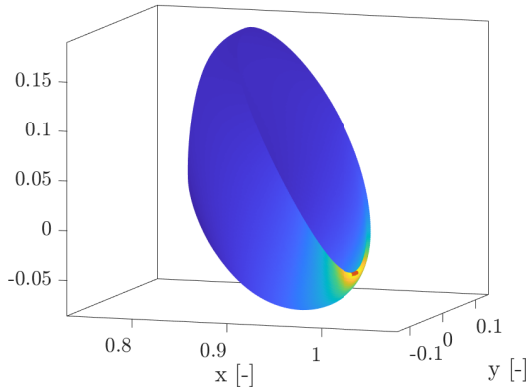


(*a*) Halo L1.

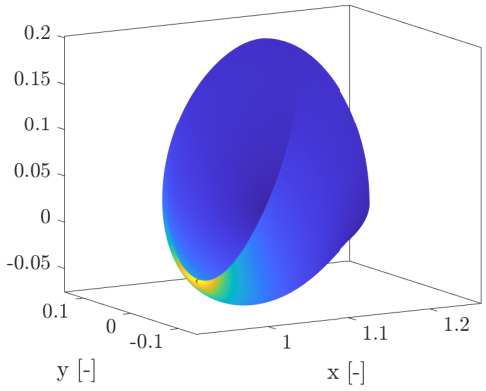


(*b*) Halo L2.

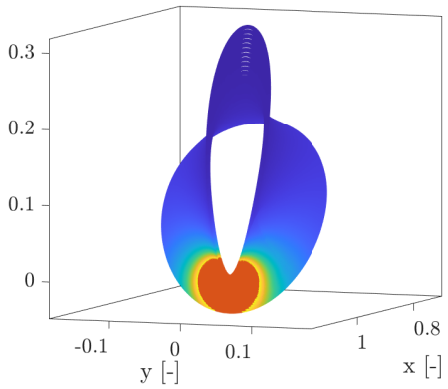


(*c*) NRHO L1.

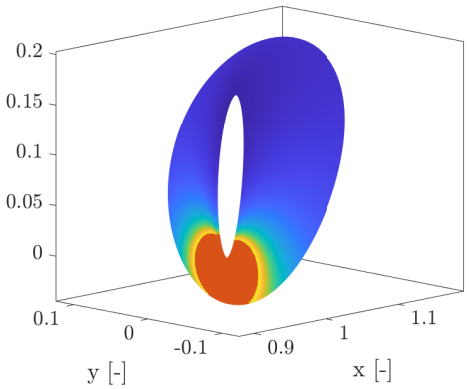


(*d*) NRHO L2.

Figure 16: Angular rate of change of $\hat{\mathbf{r}}_{T_2}$ in the CR3BP Halo and NRHO orbital families. The red markers identify the regions where the time-invariant validity threshold is violated. The color scale is associated to the same values of Fig. 14.

## 7. Conclusions

In this work the capability of a SH-MPC quasi-autonomous architecture to perform proximity operations with angles-only measurements has been extensively tested. The outcomes highlighted that in the non-keplerian dynamics, the minimisation of an observability measure based on the positive linear independence of the natural and perturbed relative position vectors generates trajectories with an extremely low degree-of-observability. In particular, it was inferred that in the cislunar space the minimisation of an objective which includes information on the range always favours a reduction of the relative distance rather than an increment on the observability angle. On the other hand, by directly targeting the angle, the guidance scheme here proposed effectively reduced the navigation error whilst remaining at relatively high distances from the target. In addition, due to its simple formulation, the optimisation problem resulted computationally efficient, with solving times in the order of fractions of a second. Finally, the analysis on the applicability of this model allowed to define critical regions in proximity of the Moon where rendezvous operations are unfeasible regardless of the propagation method, such as the NRHO and L1/L2 Lyapunov perilunes.

## References

[1] D. C. Woffinden and D. K. Geller. “Observability criteria for angles-only navigation”. In: *IEEE Transactions on Aerospace and Electronic Systems* 45.3 (2009), pp. 1194–1208.

[2] J. Grzymisch and W. Fichter. “Observability criteria and unobservable maneuvers for in-orbit bearings-only navigation”. In: *Journal of Guidance, Control, and Dynamics* 37.4 (2014), pp. 1250–1259.

[3] D. C. Woffinden and D. K. Geller. “Optimal orbital rendezvous maneuvering for angles-only navigation”. In: *Journal of guidance, control, and dynamics* 32.4 (2009), pp. 1382–1387.

[4] J. Grzymisch and W. Fichter. “Analytic optimal observability maneuvers for in-orbit bearings-only rendezvous”. In: *Journal of Guidance, Control, and Dynamics* 37.5 (2014), pp. 1658–1664.

[5] J. Grzymisch and W. Fichter. “Optimal rendezvous guidance with enhanced bearings-only observability”. In: *Journal of Guidance, Control, and Dynamics* 38.6 (2015), pp. 1131–1140.

[6] S. Mok, J. Pi, and H. Bang. “One-step rendezvous guidance for improving observability in bearings-only navigation”. In: *Advances in Space Research* 66.11 (2020), pp. 2689–2702.

[7] S. Silvestrini, J. Prinetto, G. Zanotti, and M. Lavagna. “Design of Robust Passively Safe Relative Trajectories for Uncooperative Debris Imaging in Preparation to Removal”. In: *2020 AAS/AIAA Astrodynamics Specialist Conference*. Virtual Lake Tahoe, United States, 2020, pp. 1–18.

[8] L. Bucci, A Colagrossi, and M. Lavagna. “Rendezvous in lunar near rectilinear halo orbits”. In: *Advances in Astronautics Science and Technology* 1.1 (2018), pp. 39–43.

[9] A. Colagrossi and M. Lavagna. “Cislunar Non-Keplerian Orbits Rendezvous & Docking: 6DOF Guidance and Control”. In: *69th International Astronautical Congress (IAC 2018)*. International Astronautical Federation, IAF. Bremen, Germany, 2018, pp. 1–18.